Anvil Characteristics as Seen by C-POL during the Tropical Warm Pool International Cloud Experiment (TWP-ICE)

KAYCEE FREDERICK AND COURTNEY SCHUMACHER

Department of Atmospheric Sciences, Texas A&M University, College Station, Texas

(Manuscript received 27 October 2006, in final form 21 March 2007)

ABSTRACT

The Tropical Pacific Warm Pool International Cloud Experiment (TWP-ICE) took place in Darwin, Australia, in early 2006. C-band radar data were used to characterize tropical anvil (i.e., thick, nonprecipitating cloud associated with deep convection) areal coverage, height, and thickness during the monthlong field campaign. The morphology, evolution, and longevity of the anvil were analyzed, as was the relationship of the anvil to the rest of the precipitating system.

The anvil was separated into mixed (i.e., echo base below 6 km) and ice-only categories. The average areal coverage for each anvil type was between 4% and 5% of the radar grid. Ice anvil thickness averaged 2.8 km and mixed anvil thickness averaged 6.7 km. Areal peaks show that mixed anvil typically formed out of the stratiform rain region. Peak production in ice anvil usually followed the mixed anvil peak by 1–3 h. Anvil typically lasted 4–10 h after the initial convective rain area peak. TWP-ICE experienced three distinct regimes: an active monsoon, a dry monsoon, and a break period. During the experiment (except the active monsoon period) there was a strong negative correlation between ice anvil thickness and ice anvil height, a strong positive correlation between ice anvil area and thickness, and a greater variance in ice anvil bottom than ice anvil top. These results have important implications for understanding how anvil affects the tropical atmosphere.

1. Introduction

Cirrus clouds cover up to 70% of the tropics and have a major impact on the atmospheric radiative balance and hence global climate (Liou 2002). While it is still unknown how much of the cirrus comes from deep convection, some studies have made attempts to determine this amount. For example, Massie et al. (2002) calculated 5-day back trajectories of isentropic parcels from the Halogen Occulation Experiment (HALOE) over the Maritime Continent from 1995 to 2000 and estimated that half of the cirrus formed from convective blow-off. While we lack a concrete notion of how much cirrus is formed from deep convection across the tropics, it is assumed to be significant. This study focuses on analyses of macroproperties of thick tropical cirrus still attached to or recently produced by its convective source, hereafter referred to as anvil. C-band radar data

from the Tropical Pacific Warm Pool International Cloud Experiment (TWP-ICE) that occurred in Darwin, Australia, in early 2006 were used to characterize tropical anvil areal coverage, height, and thickness during the monthlong field campaign.

Hydrometeors are generated and lofted to upper levels by deep convection. With updrafts exceeding several meters per second, some of these upper-level hydrometeors grow by riming and fall out as convective precipitation (Houze 1993). The remaining snow and ice hydrometeors can be advected into an adjacent stratiform cloud region or be left aloft in the decaying convective cell. These regions have substantially weaker vertical motions than the vigorous deep convection. Hydrometeors grow by vapor diffusion as they slowly sink in the weaker updrafts, eventually melting and precipitating out as stratiform rain. In both of these scenarios, some hydrometeors can remain aloft to form anvil. In a strong updraft situation, small precipitation-sized particles may be lifted to the level of neutral buoyancy and then spread out (because of continuity) to form anvil (Folkins 2002; Mullendore et al. 2005). In a weaker updraft situation, snow or small ice particles

Corresponding author address: Kaycee Frederick, Department of Atmospheric Sciences, Texas A&M University, 3150 TAMU, College Station, TX 77843-3150.
E-mail: kayceef@neo.tamu.edu

may simply be left aloft after the parent convective or stratiform rain regions have moved away or dissipated. Upper-level shear can also advect particles away from the precipitating regions in both scenarios. The horizontal and vertical extent of the resultant anvil depends on a number of factors, such as the duration and intensity of the initial convection, upper-level wind shear and moisture, and radiative interactions. Anvil is important to the global energy balance because it is able to persist for an extended period of time, even after its parent convection has died.

The persistence of anvil in the atmosphere can lead to changes in the radiative balance throughout the atmosphere. First, anvil will tend to increase the amount of solar radiation that is reflected back into space, thus cooling the atmosphere, but increased solar absorption within the anvil may heat the atmosphere locally. Second, anvil will decrease the amount of infrared radiation that is lost to space, thus warming the atmosphere, but infrared emission at cloud top may cool the atmosphere locally. The degree to which different heights of the atmosphere are cooled and heated by the presence of anvil across the tropics remains unknown or only very roughly estimated.

Webster and Stephens (1980) studied thick middle- and upper-tropospheric cloud during the Winter Monsoon Experiment (WMONEX) over the Malaysian region using data from the Geostationary Meteorological Satellite (GMS). With the cloud and atmospheric data obtained from WMONEX, they calculated the net radiative heating profiles for cloud layers between 350–200 and 600–200 hPa. In both cloud layers, the combined shortwave and longwave radiative effects produce a net warming of 5–10 K day^{-1} through much of the cloud. They proposed that this warming would partially maintain the cloud via lifting. Calculations from Ackerman et al. (1988) for higher, thinner cirrus clouds agree showing that, on average, infrared and solar radiation exchange heats tropical anvil.

Most numerical representations of diabatic heating processes focus on latent heating instead of radiative heating. Webster and Stephens (1980) argue that when calculating diabatic heating fields in the tropics, radiative effects cannot be ignored. This argument is especially relevant in the tropics where cloud radiative forcing (CRF)—that is, the difference between net irradiances measured with clouds and in the absence of clouds—represents the largest contribution to the total diabatic heating after latent heating (Houze 1982; Sherwood et al. 1994; Bergman and Hendon 2000). In the anvil, where vertical motions are much weaker (Mace et al. 2006), latent heating would be a secondary factor

in the total diabatic heating compared to the radiative heating. Some studies have shown the importance of including radiative effects from tropical anvil and cirrus in global models (Randall et al. 1989; Slingo and Slingo 1991; Sherwood et al. 1994). For example, Sherwood et al. (1994) demonstrated that general circulation models (GCMs) have weaker Hadley and Walker circulations when the radiative heating associated with tropical anvil and cirrus is excluded. While their GCM-reproduced TOA cloud radiative forcing compared reasonably well to satellite observations, the model assumptions about the vertical structure of radiative heating remain untested due to the lack of observations. This study takes an observational approach in investigating the possible radiative effects of anvil, including their vertical variations, by using C-band radar data collected during the TWP-ICE campaign.

Not only will statistics on tropical anvil help us to understand the atmospheric radiative budget, they will help us to quantify the atmospheric water budget as well. Figure 1 is a schematic developed around the mathematical framework introduced in Houze et al. (1980). The water budget equations developed by Houze et al. are as follows:

$$C_{\mathrm{cu}} = R_c + E_{\mathrm{cd}} + E_{\mathrm{ce}} + C_T, \tag{1}$$

$$C_T + C_{\mathrm{su}} = R_s + E_{\mathrm{sd}} + E_{\mathrm{se}}. \tag{2}$$

These equations relate the efficiency of the precipitation process to the amounts of condensate left aloft and/or injected into the large-scale environment by precipitating cloud systems. The terms in the budget include the amount of convective region condensation (C_{cu}) and the portions of the convective region condensation that are rained out (R_c), evaporated in the convective downdrafts (E_{cd}), detrained to an anvil (E_{ce}), and transported into the stratiform region (C_T). The condensate of the stratiform region includes C_T plus the amount of condensate generated by the stratiform updraft (C_{su}). Part of ($C_T + C_{\mathrm{su}}$) is rained out (R_s), part is evaporated into the downdraft (E_{sd}), and part (E_{se}) is detrained or left aloft in a mixed or iced anvil. Measurements of the anvil thickness (ΔZ_A) and areal extent (ΔX_A) can be used to better constrain E_{ce} and E_{se}.

Understanding how the anvil interacts with the rest of the precipitating system is crucial for understanding the water budget itself. Better estimates of E_{se} and E_{ce} will lead to better estimates of precipitation efficiencies, which are necessary to relate rain amounts to the vertical distribution of latent heat release. Past studies (Leary and Houze 1980; Gamache and Houze 1983) have made advances in quantifying water budget variables within the convective and stratiform regions. This

FIG. 1. Schematic vertical cross section of convective and stratiform precipitation regions and nonprecipitating anvil. This schematic was adapted from Houze et al. (1980) and has been further modified to include regions of mixed and ice anvil. Variables are defined in the text.

study is the first to make advances in quantifying the anvil terms by determining the horizontal and vertical dimensions of the ice anvil and mixed anvil regions. This study will also determine the horizontal dimensions of the convective rain (ΔX_C) and stratiform rain (ΔX_S) regions during TWP-ICE.

TWP-ICE provided a comprehensive dataset with observations from instruments such as precipitation radar, cloud radar, lidar, radiosonde, and aircraft probes. This research focuses primarily on the precipitation radar data and will attempt to quantify the horizontal and vertical dimensions of anvil regions of deep convective systems, analyze the interaction between the anvil and the rest of the precipitating system, and determine the evolution and longevity of the anvil in an attempt to better understand the radiation and water budget of tropical cloud systems.

2. Data and methodology

a. Tropical Warm Pool International Cloud Experiment

TWP-ICE, a joint venture between the U.S. Department of Energy (DOE) Atmospheric Radiation Measurement (ARM) project and the Australian Bureau of Meteorology (BOM), was held in Darwin, Australia

(Fig. 2), from 19 January to 14 February 2006 during the Australian monsoon. The wet season in Darwin is considered to occur from 1 October to 30 April (Hastenrath 1991), and, in particular, the Australian monsoon season generally lasts from December to March.

FIG. 2. Map of the TWP-ICE region. Sounding stations are represented by triangles. The thick solid circles indicate the 120-km radius from C-POL.

The Australian monsoon is associated with the inflow of moist west-to-northwesterly winds, originating from the Indian Ocean, into the monsoon trough. The monsoon produces convective activity leading to large amounts of rainfall (monthly averages between 400 and 600 mm) over northern Australia. During TWP-ICE, an intense airborne measurement campaign was combined with an extensive network of ground-based observations to describe the evolution of tropical convection. TWP-ICE had a dual focus in being designed to study the characterization of cirrus and the upper troposphere along with the convective environment.

Cloud properties during this experiment were observed by an extensive set of in situ and remote sensing instruments. A map of the experiment area is shown in Fig. 2. A fleet of five aircraft flew in the boundary layer and at multiple cloud levels. The Darwin ARM site, which is located in Darwin for long-term climatological observations, retrieved a comprehensive set of passive and active radiation measurements, including observations using a micropulse lidar and a 35-GHz millimeter-wave cloud radar (MMCR). A similar set of instruments located on the research vessel (R/V) *Southern Surveyor* offshore of Darwin provided for oceanic measurements. Other surface measurements included two scanning, C-band Doppler radars [the C-band polarimetric/Doppler meteorological radar system (C-POL) and the operational radar in Darwin], wind profilers, surface flux stations, and a network of five radiosonde stations encircling Darwin. Radiosondes were launched every 3 h providing very high temporal resolution. More details on the instrumentation during TWP-ICE can be found in the Science Plan (online at www.bom.gov.au/bmrc/wefor/research/twpice.htm).

b. C-band polarimetric/Doppler meteorological radar system

C-POL was developed by modifying a standard operational C-band radar employed by the Australian Bureau of Meteorology to be able to transmit linear horizontal and vertical polarizations and to receive the co- and cross polarizations on a pulse-to-pulse basis (Keenan et al. 1998). C-POL has a 1.0° beamwidth. Assuming no path attenuation, the minimum detectable reflectivity at 10 km is -29 dBZ. At further distances, the sensitivity decreases so a minimum reflectivity of 0 dBZ is employed in this work. Because C-band measurements attenuate in heavier rain, the polarimetric measurements are used in C-POL's attenuation correction. The C-POL volume scan strategy during TWP-ICE consisted of 17 tilts using the follow-

ing angles: 0.5°, 1.2°, 1.9°, 2.6°, 3.5°, 4.4°, 5.3°, 6.4°, 7.8°, 9.6°, 11.7°, 14.3°, 17.5°, 21.4°, 26.1°, 33°, and 42°.

C-band radar is suitable for studying thick anvil because it transmits and receives at a 5-cm wavelength. In general, this is a short enough wavelength to allow for measurements of smaller hydrometeors as compared to a S-band (~10-cm wavelength) radar, but is a long enough wavelength not to be attenuated during heavy precipitation like a cloud radar (i.e., a millimeter-wavelength radar).[1] C-POL is a scanning radar so it can cover much larger areas (typically a 140-km radius from the radar) than a vertically pointing cloud radar. Although sensitivity studies have yet to be completed, Fig. 3 presents a visual comparison of the vertically pointing cloud radar (MMCR) and the precipitation radar. At 0700 UTC, C-POL sees anvil ~2 km thick while the MMCR sees anvil that is ~3 km thick. At 1130 UTC, the precipitation radar sees anvil ~3.5 km thick while the cloud radar sees anvil that is ~4.5 km thick. It appears then, on average, that C-POL only misses about 1 km of the anvil compared to what is observed by the more sensitive MMCR. However, McGill et al. (2003) showed that a highly sensitive cloud radar still misses some of the anvil top. Another point to take into consideration is that the MMCR suffered a loss of sensitivity due to a lightning strike just before the TWP-ICE campaign. From this information, it is hard to tell how much of the anvil C-POL is actually missing, but it is potentially greater than a kilometer. Finally, it should be noted that C-POL reflectivity measurements cannot discriminate between hydrometeors that are in suspension and hydrometeors that are falling as precipitation.

The raw data collected from C-POL was converted to universal format (UF). In this step, signal processing was performed to remove some of the ground clutter. Next, principles from Bringi et al. (2001) were used to calculate polarimetric variables and correct for attenuation. Then a quality control method developed by the University of Washington (Houze et al. 2004) was used to remove pervasive clutter. This quality control method examines the texture of the reflectivity field in both the horizontal and vertical to determine which gates are set to missing data. In the final step, the polar data were interpolated to a Cartesian grid (2 km × 2 km in the horizontal and 0.5 km in the vertical) using National Center for Atmospheric Research (NCAR) Reorder. The radius of influence used by Reorder was 2 km in the x and y dimensions and 1 km in the z dimension. Finally, data outside a radius of 120 km

---

[1] Other variables in the radar equation are important to consider. See Keenan et al. (1998) for other C-POL characteristics.
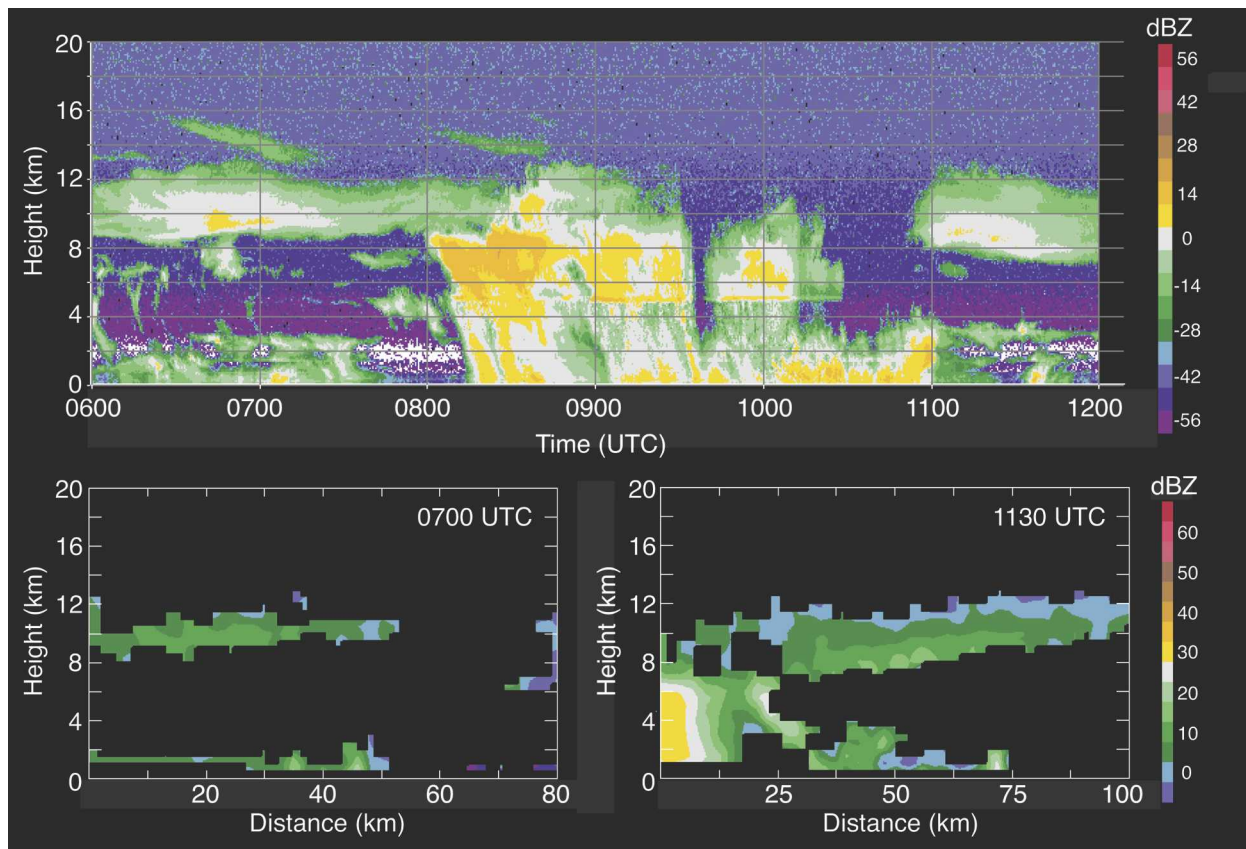
FIG. 3. Comparison of precipitation radar (C-POL) and cloud radar (MMCR) observations over the ARM site on 24 Jan 2006. (top) Cloud radar reflectivity from 0600 to 1200 UTC. (bottom left) Precipitation radar reflectivity at 0700 UTC and (bottom right) precipitation radar reflectivity at 1130 UTC. The ARM site is in the middle of the precipitation radar cross sections. Images courtesy of J. Cetrone.

from the radar (Fig. 2) were excluded from the analysis because pervasive clutter still remained at upper levels far away from the radar.

c. Analysis of C-POL data

Once the C-POL data were quality controlled, echo characteristics during TWP-ICE were analyzed using the 3D reflectivity arrays from the Cartesianized C-POL data. Anvil was defined as echo aloft (i.e., tops at or above 6 km MSL) that had no reflectivity measurements at 2.5 km MSL. Anvil top was determined by starting at the top of a given reflectivity profile and searching downward until a data value was found. This was then defined as the anvil top. The same method was used for anvil bottom except the search started from the bottom up. Anvil thickness was determined by subtracting anvil bottom from anvil top. Note that this method of defining the anvil cannot discriminate anvil located over shallow convection reaching 2.5 km MSL (radar clutter below 2.5 km MSL, which is evident in the bottom panels of Fig. 3, will not affect the anvil

calculations); however, visual observations show minimal occurrences of this situation so these events should not be statistically significant.

Next, the anvil was separated into ice anvil and mixed anvil subcategories. Regions a and b of Fig. 4 show an example of these two subcategories, respectively. Ice anvil was defined as anvil that has a base no lower than 6 km, which in the tropics would be around $-5°C$ thus assuring that most of the hydrometeors in the anvil above this level would be ice. All other anvil was considered mixed anvil, indicating a mix of water and ice hydrometeors. Anvil area was calculated summing the pixels in the anvil thickness arrays in the x and y dimensions. The importance in separating these two regions is that clouds composed of ice versus clouds composed of ice and liquid have different impacts on the atmospheric radiative balance and convective system water budget (Houze 1982; Ackerman et al. 1988).

Houze (1997) points out that convective and stratiform precipitation are produced from dynamically different situations. Convective rain is produced from col-
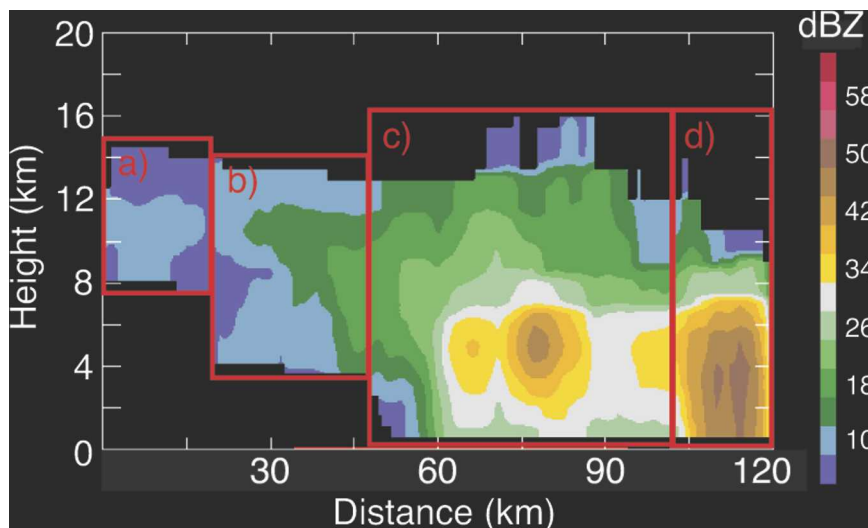
FIG. 4. Vertical C-POL cross section at 1800 UTC 31 Jan 2006 of (a) ice anvil, (b) mixed anvil, (c) stratiform rain, and (d) convective rain regions.

lection processes indicating strong vertical motion. Hydrometeor growth in the stratiform rain region is produced by vapor diffusion because of the weaker vertical motions. Regions c and d of Fig. 4 shows examples of stratiform and convective rain regions, respectively. To distinguish between these dynamically different regions, surface rain (i.e., echo observed at 2.5 km) was separated into convective and stratiform regions using the algorithm from Steiner et al. (1995). This method analyzes horizontal gradients in radar reflectivity to distinguish regions of convective precipitation from stratiform precipitation. More peaked echo is classified as convective and the remaining echo is classified as stratiform. As a further criteria, any pixel with reflectivity greater than 40 dBZ (or $\sim$10 mm h^{-1}) is automatically considered convective. Once reflectivity was separated into convective and stratiform components, the same methods used to find anvil top were used to find convective and stratiform top. The number of pixels in the convective and stratiform top arrays was then summed to give convective and stratiform rain areas.

3. Results

The following section discusses radar data analyzed from 19 January to 11 February 2006. During TWP-ICE there were three distinct weather regimes: 19 January through 25 January was classified as the active or "wet" monsoon. This regime was characterized by westerly monsoon flow and large mesoscale convective systems (MCSs). From 26 January through 2 February was classified as the "dry" monsoon. During this regime the monsoon low was inland and deep, and although the westerlies were very strong during this time they

were of drier origin contributing to less convection over Darwin. From 3 February through 11 February was classified as the "break" period. During this time, the monsoonal trough had moved out of the region and an inland heat trough dominated northern Australia accompanied with easterly winds. Storms formed along both trough and sea-breeze boundaries and often came in the form of squall lines. Two days from each regime were selected as case studies, three of which are discussed in this paper. Statistics encompassing the entire TWP-ICE campaign were analyzed as well.

a. Case studies

1) ACTIVE MONSOON: 24 JANUARY

The radar domain during 24 January experienced a great deal of convective activity. The edge of a rotating MCS was inside the radar domain early this day, producing a large amount of stratiform rain. Later in the day, a large squall line moved eastward through the domain.

A large convective system was present in the western part of the radar domain at 0200 UTC (1130 Darwin LT), which produced a large area of stratiform and convective rain with echo tops above 10 km and very little mixed or ice anvil (Figs. 5a, 5b, and 6). Most of the convection had moved west out of the area by 1100 UTC (Figs. 5c and 6). Figures 5d and 6 indicate a large region ($\sim$25% of the radar domain[2]) of anvil at 10 km left behind by the MCS. Figure 6 shows that much of

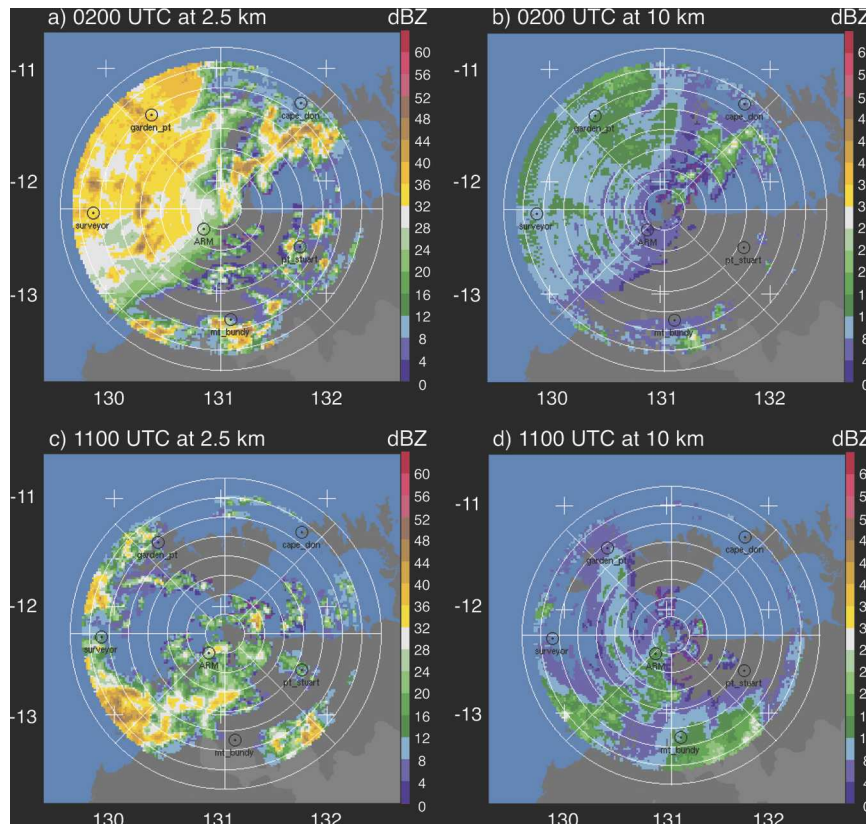---

[2] The area of the radar grid is 45 216 km^2.

Fig. 5. C-POL horizontal cross sections on 24 Jan 2006 at (a) 0200 UTC at 2.5 km MSL, (b) 0200 UTC at 10 km MSL, (c) 1100 UTC at 2.5 km MSL, and (d) 1100 UTC at 10 km MSL. Range rings are every 20 km.

this echo aloft was ice anvil and that ice anvil covered 15%–20% of the radar domain for roughly 10 h (i.e., between 0500 and 1500 UTC). Mixed anvil also covered ~15% of the radar domain at 0500 UTC, but decreased in coverage over the next 10 h. A new convective system moved in from the west starting at 1600 UTC (Fig. 6). This new system caused ~50% of the radar grid to be covered by stratiform rain with a concurrent peak in convective rain area. The convective and stratiform rain area peaks were followed by first a peak in mixed anvil and then a peak in ice anvil at 2–3-h intervals. These lags in area will be discussed in further detail in section 4. Average anvil height and thickness did not vary much on this day (Fig. 7). Ice anvil average tops remained around 12 km while ice anvil thickness was about 4–5 km. Mixed anvil was 7 km thick on average throughout the day and had average tops around 11 km.

2) Dry monsoon: 1 February

Convective activity was more suppressed compared to the wet monsoon during this time period of strong westerlies. Most of the convective activity on 1 February came in the form of fast-moving squall lines, as opposed to large MCSs.

Figures 8a and 8b show an eastward-moving squall line inside the radar domain at 0200 UTC with a limited amount of echo at 10 km, some of which is indicative of anvil behind the convective line. Convective rain area peaked at this time and the stratiform rain, mixed anvil, and ice anvil areas increased over the next 1–3 h (Fig. 9). Although ice anvil area was still relatively limited during this period, the ice anvil that was present had an average thickness of 3 km after the convective peak (Fig. 10). Mixed anvil was consistently 5–6 km thick.

Stratiform rain area peaked at 0300 UTC (Fig. 9) as a second line moved in from the west and the previous line became more stratiform in nature. A peak in mixed anvil area occurred shortly after the peak in stratiform rain area implying a link between stratiform rain and mixed anvil production. This same lag is seen again when the line that entered the radar domain at 0300 UTC and a third squall line that entered the domain at 0500 UTC moved through the northern part of the ra-
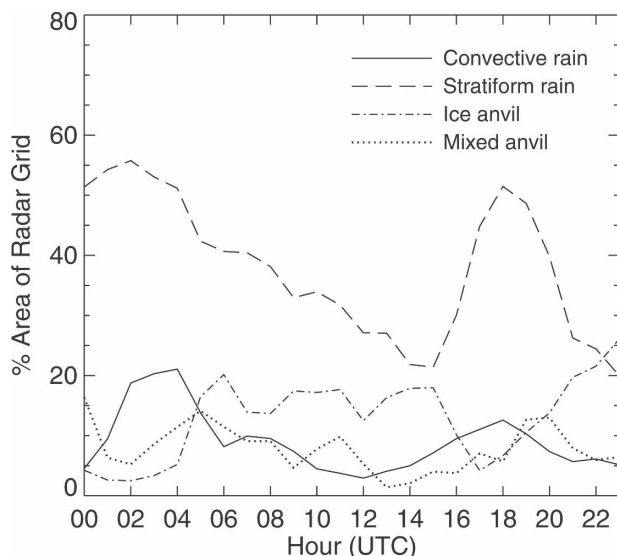
FIG. 6. Percentage of radar grid covered by rain and anvil on 24 Jan 2006.

dar domain. Stratiform rain area peaked again at 0600 UTC as the rapidly moving squall lines became more stratiform in nature (Figs. 8c and 8d), with a maximum in mixed anvil area lagging 1–2 h behind followed by a peak in ice anvil at 1000 UTC (Fig. 9). As stated before, this lag will be elaborated on in the discussion section of this paper.

By 0800 UTC convection was well on its way out of the radar domain, but the series of squall lines left a good portion of anvil in the atmosphere. Total anvil area coverage of 10%–20% lasted for about 4 h past 0800 UTC (Fig. 9). From 1400 to 1600 UTC small areas of convection were present, which added to the production of anvil. Although the coverage was smaller (5%–10%), anvil was still present until 1600 UTC after which most of the anvil either advected off the domain or

dissipated. The ice anvil average top was around 13 km and average thickness was around 3 km on this day with little variation between 0200 and 1700 UTC (Fig. 10). These values indicate higher, thinner ice anvil than the active monsoon case. Mixed anvil top height was also steady with an average top around 10 km and average thickness around 6 km (Fig. 10), slightly lower than the values seen during the active monsoon case.

3) BREAK PERIOD: 10 FEBRUARY

Typical for the break period, 10 February experienced times of moderate convective activity. Hectors, defined as convection forming over the Tiwi Islands in the afternoon, were common during the break period. In addition to hector, convective activity on 10 February came in the form of two westward-moving squall lines. The convection on this day appeared to be more favorable for ice anvil production than during the other two periods.

The first peak in convective rain area was associated with a hector that formed around 0600 UTC (Fig. 12). Ice anvil thickness increased to 5 km by 0700 UTC (Fig. 13), which is about 2.5 km above average for the break period (Table 1). Ice anvil stayed at this average thickness for several hours. As the ice anvil thickness increased, the ice anvil also began to sink (Fig. 13). The ice anvil top averaged 15 km at 0500 UTC and 13 km at 1500 UTC, while the ice anvil bottom showed a larger decrease. The processes contributing to this sinking will be discussed further in section 4. Even though mixed anvil area was small, the mixed anvil that was present was unusually thick at 10 km (Fig. 13), which is about 5 km above average for this regime (Table 1). The average mixed anvil top reached 15 km during this time. The higher anvil tops during this day are indicative of the deeper convection during the break period.
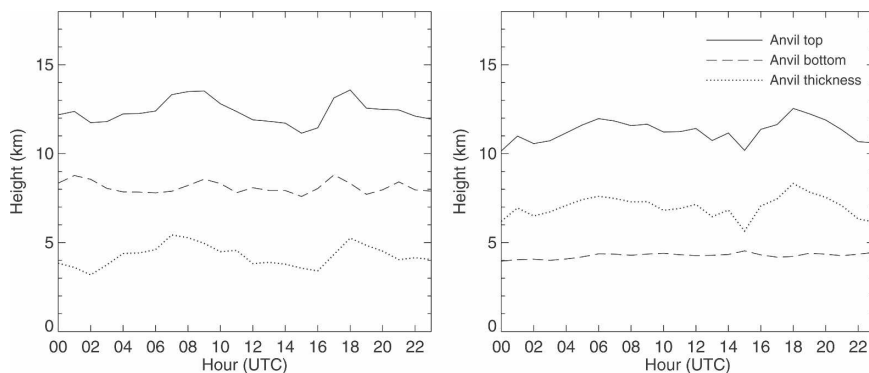
Around 0800 UTC, the hector convection weakened

FIG. 7. Average anvil top, bottom, and thickness for (left) ice anvil and (right) mixed anvil on 24 Jan 2006.
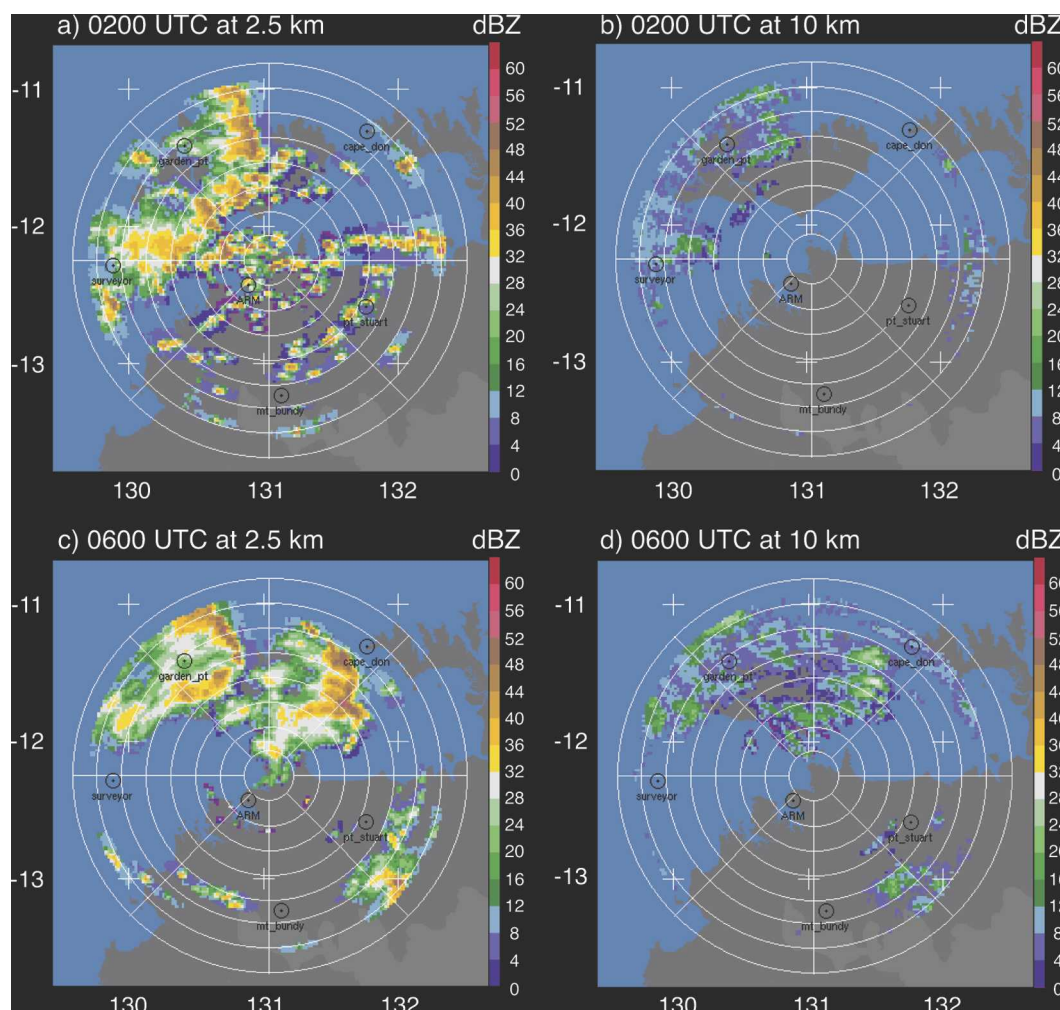
FIG. 8. C-POL horizontal cross sections on 1 Feb 2006 at (a) 0200 UTC at 2.5 km MSL, (b) 0200 UTC at 10 km MSL, (c) 0600 UTC at 2.5 km MSL, and (d) 0600 UTC at 10 km MSL. Range rings are every 20 km.

and moved northwestward while producing a moderate anvil region at 10 km, most of which was ice anvil (Figs. 11a, 11b, and 12). By 1100 UTC, the echo associated with the hector had advected off of the radar domain and a convective system with some stratiform rain had moved into the domain from the south (Fig. 12). Within a couple of hours this squall line produced a very large area of both mixed and ice anvil (Figs. 11c, 11d, and 12). Not only was the anvil large in areal extent, but it was quite thick for the break period (Fig. 13; Table 1). Despite the anvil's thickness, it was not as long lived as in the active monsoon case and dissipated within approximately 4 h after initial peak in area. This shorter lifetime could be due to the upper atmosphere being drier during this regime or that there was simply less large hydrometeors lofted into the atmosphere by this type of convection (e.g., because of shorter-lived convection or convection with a higher precipitation efficiency).

A second squall line moved through the radar domain around 2100 UTC. Figure 12 shows a peak in convective rain area followed by a larger peak in stratiform area a couple hours later. The squall line left some ice anvil behind, but mixed anvil was gone by 0300 UTC the next day. The ice anvil that was produced from this system exhibited an increase in thickness around 0300 UTC the next day, but only lasted about an hour or two before being advected off the radar domain or dissipating.

b. Entire field experiment

1) RAIN AND ANVIL AREA

The percent of the radar grid covered by ice anvil, mixed anvil, convective rain, and stratiform rain during TWP-ICE is shown in Table 2. The table is also broken down by regime. The experiment average of area cov-
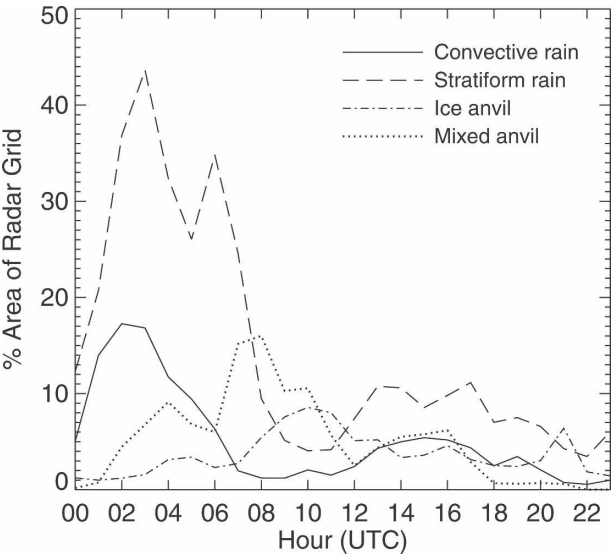
FIG. 9. Percentage of radar grid covered by rain and anvil on 1 Feb 2006.

TABLE 1. Average values for anvil properties during TWP-ICE.

	Ice	Mixed
Thickness (km)		
Experiment	2.8	6.7
Active	4.0	6.6
Dry	2.1	6.1
Break	2.5	7.6
Top (km)		
Experiment	14.5	10.9
Active	12.4	10.8
Dry	14.9	10.3
Break	15.5	11.8
Bottom (km)		
Experiment	11.7	4.2
Active	8.4	4.2
Dry	12.7	4.2
Break	12.9	4.2
Height (km)		
Experiment	13.1	7.5
Active	10.4	7.5
Dry	13.8	7.3
Break	14.2	8.0

erage for both anvil types and the convective rain category was between 4% and 5%, whereas stratiform rain covered 15% of the radar grid on average. Comstock et al. (2002) and Mace et al. (2006) analyzed long-term records of vertically pointing cloud radar data over two islands in the tropical west Pacific and found that high clouds (i.e., clouds with bases above 7 km) occur up to 48% of the time, although many of these high clouds were not directly linked to deep convective sources.

The largest coverage from all echo types occurred during the active period, which can also be seen in the time series in Fig. 14. During this period, ice anvil, convective rain, and stratiform rain area doubled compared to the overall experiment averages, while the mixed anvil area tripled. During the active phase,

mixed anvil covered 15.6% of the radar grid, while ice anvil covered 7.6% of the grid (Table 2). The large coverage of mixed anvil is probably linked to the significant amount of stratiform rain production during the active monsoon.

During the dry monsoon and break period, stratiform rain production was not as dominant and ice anvil covered 1%–2% more of the radar grid than mixed anvil. The anvil area was smallest during the dry period; ice anvil area averaged 2.1% and mixed anvil area averaged 1.3%. During the break period, the ice anvil area (3.6%) remained close to the experiment average while the mixed anvil area (1.7%) and convective and stratiform rain areas (2.2% and 5.6%) decreased substantially, implying that smaller convective systems
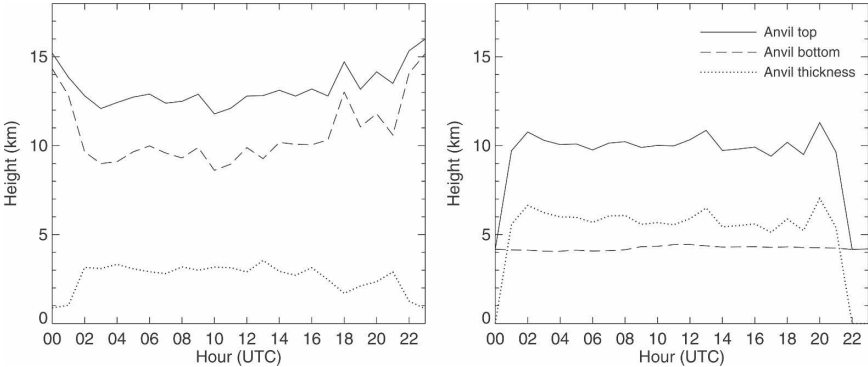

FIG. 10. Average anvil top, bottom, and thickness for (left) ice anvil and (right) mixed anvil on 1 Feb 2006.
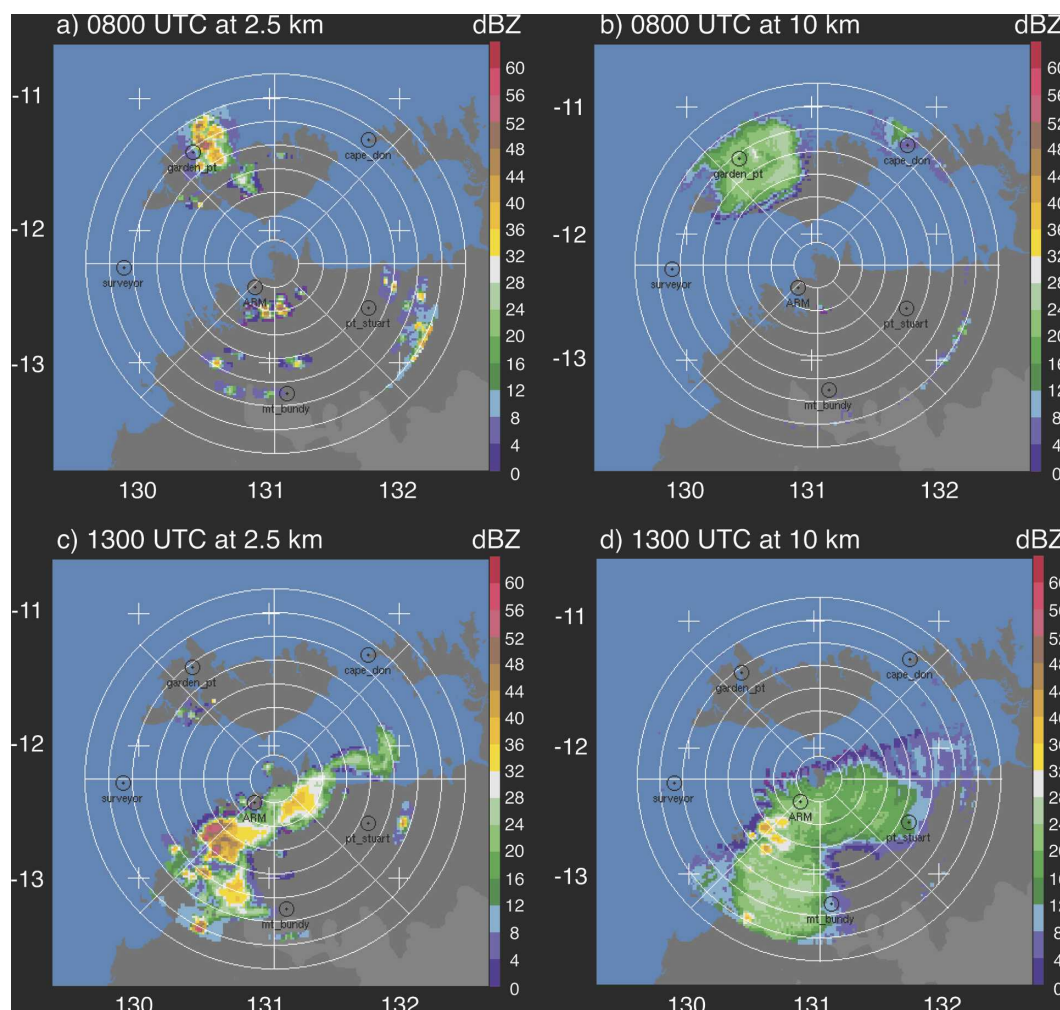
FIG. 11. C-POL horizontal cross sections on 10 Feb 2006 at (a) 0800 UTC at 2.5 km MSL, (b) 0800 UTC at 10 km MSL, (c) 1300 UTC at 2.5 km MSL, and (d) 1300 UTC at 10 km MSL. Range rings are every 20 km.

were producing proportionally large amounts of ice anvil.

2) ANVIL HEIGHT AND THICKNESS STATISTICS

Table 1 shows the average values of anvil thickness, top, bottom, and height during the whole experiment and also broken down by regime. The experiment average of ice anvil thickness was 2.8 km, which is about 1 km thicker than the average thickness of high clouds observed by Comstock et al. (2002) and Mace et al. (2006). These results are consistent since C-POL cannot sense the thinner cirrus observable by cloud radar, the inclusion of which would lower the average thickness. For mixed anvil, the experiment average thickness was 6.7 km.

During the active monsoon, ice anvil was much thicker and lower in height on average than during the dry monsoon and break period (Fig. 15). The average thickness for ice anvil during the active monsoon was 4 km, compared to 2.1 and 2.5 km during the dry monsoon and break period, respectively (Table 1). The average height (i.e., the average of anvil top and bottom) for ice anvil during the active monsoon was 10.4 km, which was lower than dry monsoon and break period mean heights of 13.8 and 14.2 km. The experiment average ice anvil mean height of 13.1 km is consistent with the high cloud heights observed by Comstock et al. (2002) and Mace et al. (2006).

Although ice anvil characteristics between the active and dry monsoon are different, mixed anvil during these two time periods show similar characteristics (Fig. 15). The average thickness only differed by 0.5 km and average heights only differed by 0.2 km (Table 1). The mixed anvil during the break period was 1–1.5 km
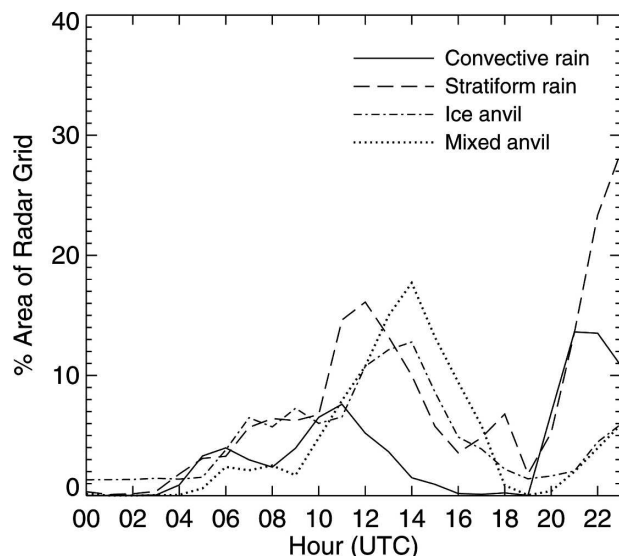
FIG. 12. Percentage of radar grid covered by rain and anvil on
10 Feb 2006.

thicker and ~0.5 km higher compared to the active and
dry monsoon.

Figures 14 and 15 imply that ice anvil thickness is
negatively correlated with ice anvil height and ice anvil
area is positively correlated with ice anvil thickness.
Calculations show a −0.9 correlation between daily ice
anvil thickness and mean height and a 0.7 correlation
for daily ice anvil area and thickness for the entire field
campaign. During the active period, the daily ice thick-
ness did not vary much. However, peaks in thickness on
1, 6, and 9 February make this negative correlation to
height (positive correlation to area) obvious during the
dry monsoon and break periods. Possible reasons for
these relationships will be addressed in the discussion
section.

Anvil height and thickness were more variable dur-

ing the break period than during the active and dry
monsoon (Table 3). Mean height variance for ice anvil
during the active and dry monsoon was 0.3 and 0.7 km
compared to 3.2 km during the break period. Ice anvil
thickness variance during the break period was 1.9 km
compared to that of 0.1 km for the active and dry mon-
soon. Mixed anvil shows similar results for height and
thickness, with most variability during the break period.
This variability is expected due to more isolated con-
vection during the break period and more organized
convective systems during the active monsoon. An-
other interesting feature in the variance is that ice anvil
bottom varied more than the ice anvil top (mixed anvil
bottom variance was 0 due to the method in which
mixed anvil is classified). There was an exception to this
type of relationship during the active period, when nei-
ther the ice anvil bottom nor top varied much. Over the
entire experiment, the ice anvil base height had a vari-
ance of 6.4 km compared to the ice anvil top height
variance of 2.3 km. This difference was even more ex-
treme during the break period when the ice anvil bot-
tom had a variance 4.9 km greater than the top. Rea-
sons for this difference will be discussed in section 4c.

4. Discussion

a. Convective pattern and longevity

Of the 12 MCSs observed in the daily case studies
(including three case study days not shown), 8 MCSs
followed a pattern in which the convective rain area
would peak first, followed by a peak in stratiform rain
area, then a peak in mixed anvil area and finally ice
anvil area (Figs. 6, 9, and 12). The peak in stratiform
area occurs within an hour of the initial convective
peak. These results are consistent with Churchill and
Houze (1984) and Houze (1997), in that stratiform rain
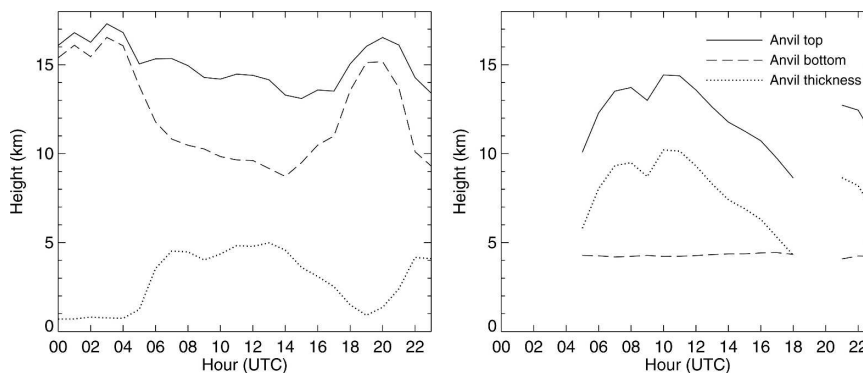is formed from aging convection; however, these stud-

FIG. 13. Average anvil top, bottom, and thickness for (left) ice anvil and (right) mixed
anvil on 10 Feb 2006.

TABLE 2. Average percent of the radar grid area covered during TWP-ICE.

	Ice	Mixed	Convective	Stratiform	Total	Rain/anvil ratio
Experiment	4	4.8	4.4	14.9	28.2	2.2
Active	7.6	15.6	8.6	33.2	65	1.8
Dry	2.1	1.3	3.9	11.9	19.3	4.6
Break	3.6	1.7	2.2	5.6	13	1.5

ies did not discuss anvil evolution in relation to the parent convection. Typically, the mixed anvil area peak would lag the stratiform area by 1–2 h. This lag implies that mixed anvil forms from and possibly at the expense of stratiform rain. A peak in ice anvil area shows up anywhere within 1 h to as late as 3 h after a peak in mixed anvil area. This could be due to upper-level shear advecting particles away from the parent convective system to form ice anvil or evaporation in the lower levels of the mixed anvil.

There were five cases in which the convective system was isolated enough to observe the longevity of the anvil. During these cases, anvil lasted 4–10 h after the initial peak in convective rain area. Since the anvil is being measured within a set domain, it is difficult to tell how much anvil is dissipating or just advecting off of the domain. Overall, the ratio of rain area to anvil area during TWP-ICE is 2.2 (Table 2). That is, there is about half as much area covered by thick anvil as is covered by rain during the Australian monsoon. This number could potentially provide a rough estimate of tropics-wide thick anvil coverage if applied to satellite observations of rain area in regions of deep convection.

b. Correlations between thickness, height, and area

In each regime, except within the active regime, and throughout the entire experiment thicker ice anvil is associated with lower heights and larger areal coverage. These correlations are evident in the daily time series of Figs. 14 and 15 and likely result from how the anvil develops and evolves over time. When a convective cell first lofts hydrometeors into the upper atmosphere, the hydrometeors usually reach a level of neutral buoyancy and begin to spread out laterally. Over time, hydrometeors accumulate aloft and increase anvil areal extent. Upper-level shear and a moist upper troposphere would assist in increasing and maintaining anvil areas. Eventually these hydrometeors sediment out, creating a thicker anvil with a lower base. The sinking of the anvil itself could occur if the larger particles that are usually found at the base of the anvil fallout first and evaporate, hydrating the environment just under the current base of the anvil. When the small particles, which are normally at the top of the anvil, sediment out

the new environment would be moist enough to sustain the particles and prevent them from evaporating. This process would cause the whole anvil to lower over time. Given an ice hydrometeor fall speed of 0.5–1.0 m s^{-1}, sedimentation could cause the anvil base to drop 2–3 km within 1 h.

Figure 16 shows C-POL observing this process. On 10 February 2006 at 1130 UTC, anvil is starting to form from a convective cell. At the anvil's initial development, its top is ~15 km with a base around 11 km. Within 30 min the majority of the anvil base is below 10 km and the top remains around 15 km. By 1230 UTC the anvil base is ~8 km, creating a thicker anvil. The top has lowered somewhat but only the portion farthest away from the convective core. An hour and a half from the initial observation, the anvil base lies slightly above 6 km with the top near or above 15 km. In addition, no reflectivity values greater than 15 dBZ are at upper levels of the anvil and reflectivity values greater than 20 dBZ are below 12 km indicating more and/or larger hydrometeors (aggregation along with sedimentation may be contributing to this signal). Also, the
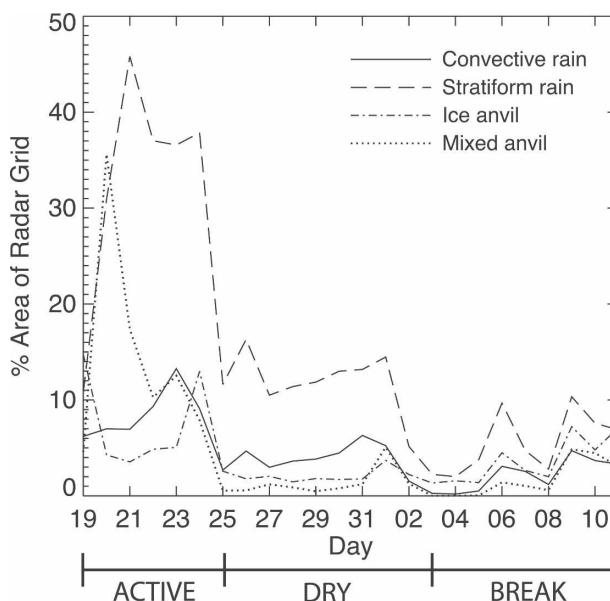

FIG. 14. Percentage of radar grid covered by rain and anvil during TWP-ICE.
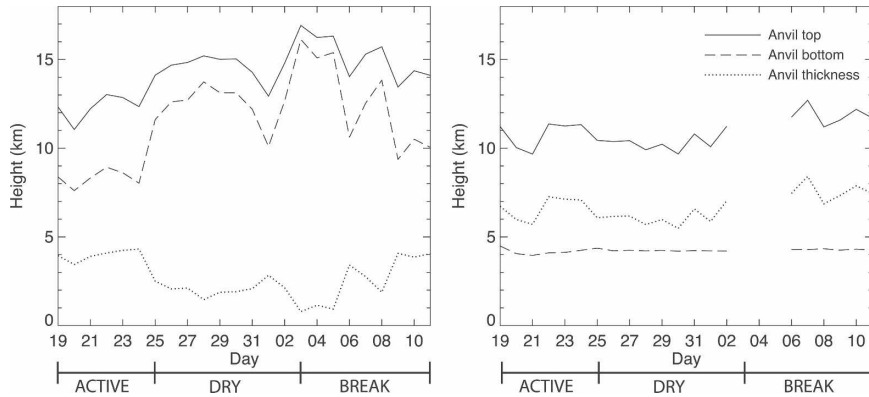
FIG. 15. Average anvil top, bottom, and thickness for (left) ice anvil and (right) mixed anvil during TWP-ICE.

anvil initially extends ~20 km from the convective core, increasing to ~55 km from the convective core with time. Thus, Fig. 16 shows that the anvil became thicker and increased in area over a period of an hour and a half. Even though the anvil top did not sink as much as the anvil bottom, the mean height of the anvil decreased due to the substantial sinking of the anvil bottom.

c. Variance in ice anvil base

The most variability in daily anvil properties was between ice anvil top and bottom (Table 3). This comparison is not useful for mixed anvil since the mixed anvil definition requiring the base to be less than 6 km does not allow for much variability in anvil bottom. Averaged over the entire experiment, the ice anvil bottom varied significantly more than the ice anvil top. When broken down by convective regimes, the same result is seen except during the active monsoon. The variance for both ice anvil top and bottom during this regime was very small due to the nature of the convection, which was wider spread and longer lived. There are a few possible physical explanations for the ice anvil bottom being more variable than the top in the other periods.

It is reasonable to assume that anvil top height is located around one or more levels of neutral buoyancy (Folkins 2002; Mullendore et al. 2005). Therefore, any type of internal buoyant motion that occurs at the anvil top will not be able to penetrate through the stable layer. Since the anvil bottom is not constricted by this stable layer, cells would have more freedom to penetrate downward. The restrictiveness of the level of neutral buoyancy could explain why Petre and Verlinde (2004), using vertically pointing cloud radar measurements, observed cells becoming more deeply embedded in the base of the anvil.

Another possible explanation is that there is increased ice water content (IWC) in the base of the anvil. McFarquhar and Heymsfield (1996) studied in situ measurements from three anvil cases during the Central Equatorial Pacific Experiment (CEPEX). Using an optical array probe they found that IWC increases downward in the anvil. The large IWC would cause a higher radiative destabilization rate (Lilly 1988) due to the absorption of radiation thus causing the anvil bottom to heat and rise. Their measurements also show that total cross-sectional area (A_c) of the cloud particles per unit volume is at least one order of magnitude larger near the base of the cloud than near the top. Again, this would lead to greater radiative destabilization in the anvil base due to more absorption and extinction of radiation in the larger particles.

TABLE 3. Variance of anvil properties during TWP-ICE.

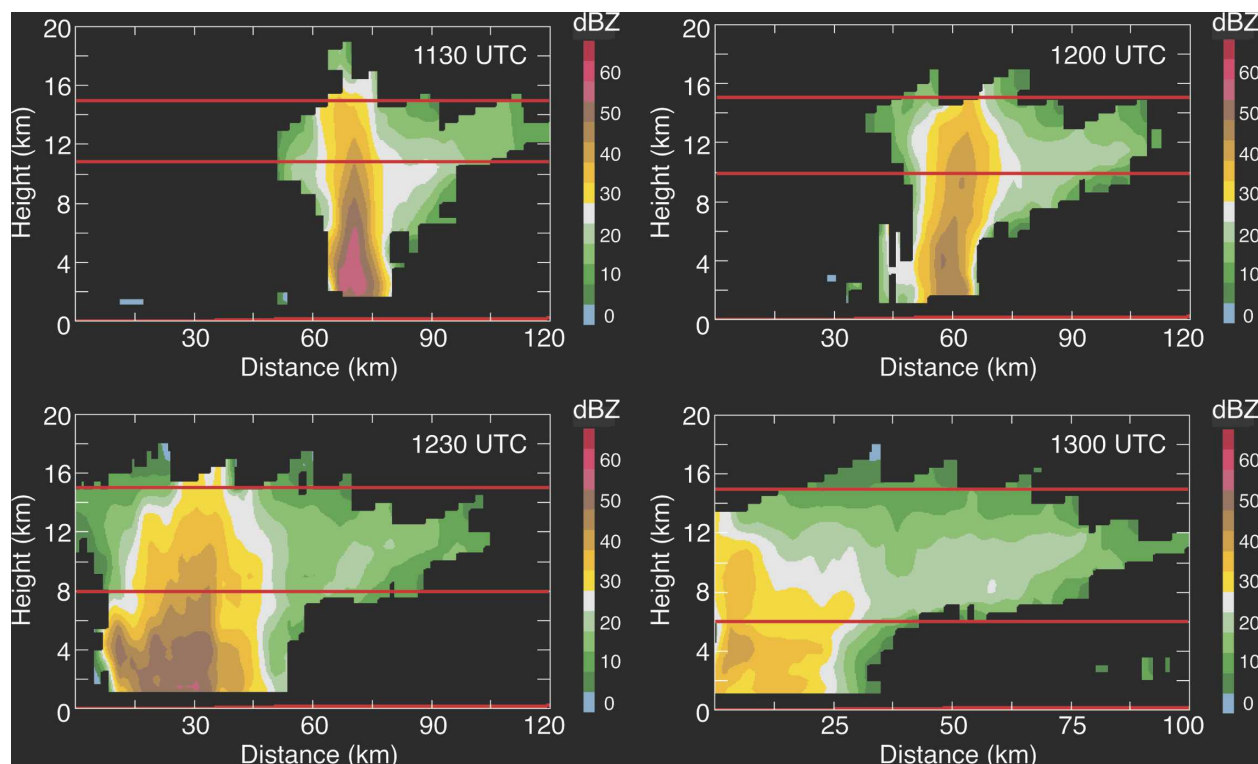|	Ice	Mixed
Thickness (km)		
Experiment	1.3	0.7
Active	0.1	0.4
Dry	0.1	0.2
Break	1.9	0.3
Top (km)		
Experiment	2.3	0.7
Active	0.5	0.6
Dry	0.5	0.2
Break	1.2	0.3
Bottom (km)		
Experiment	6.4	Null
Active	0.2	Null
Dry	1.0	Null
Break	6.1	Null
Height (km)		
Experiment	4.0	0.7
Active	0.3	0.2
Dry	0.7	0.1
Break	3.2	3.8

FIG. 16. A series of vertical cross sections from 1130–1300 UTC 10 Feb 2006. This series shows the sedimentation process occurring in the anvil.

As discussed in section 4b, sedimentation would contribute to the variance of the anvil bottom. Variance may also occur in the anvil base as large ice crystals fall into a dry layer near cloud base and then sublimate (Heymsfield and Miloshevich 1995). For example, mammatus clouds that form from the cooling of the air as precipitation particles fall and evaporate could also cause some of the observed variance.

5. Conclusions

The horizontal and vertical dimensions of the anvil region (i.e., the thick, nonprecipitating cloud directly associated with deep convection) can be used to help determine the radiative impact and better quantify the water budget of tropical convective systems. The experiment averages of area coverage for mixed and ice anvil were between 4% and 5% (or 8.8% total) of the radar grid. Because of the robust nature of the convection, the largest anvil areal coverage occurred during the active monsoon with ice anvil covering 7.6% of the radar grid and mixed anvil covering 15.6% of the grid. Because of the relatively small amount of convection and its more shallow nature, the least amount of anvil was produced during the dry monsoon; ice and mixed anvil covered 2.1% and 1.3% of the radar grid, respectively. Break period ice anvil coverage was closer to the experiment average at a value of 3.6% while the mixed anvil area decreased to only 1.7% of the radar grid. Ice anvil thickness was 2.8 km and mixed anvil thickness was 6.7 km averaged over the experiment. The thickest ice anvil was produced during the active monsoon, with ice anvil thickness averaging 4 km, compared to only 2.1 and 2.5 km during the dry monsoon and break period, respectively. Because of higher convective cloud tops, the thickest mixed anvil was produced during the break period with an average thickness of 7.6 km, compared to 6.6 and 6.1 km during the active and dry monsoon. Applying these results to Fig. 1 will help to quantify the pictured water budget (Fig. 17).

Since parent convection is likely of first-order importance in determining anvil height, thickness, and areal coverage, it is important to show how anvil evolves from the parent convection and how long the anvil persists. Eight out of the twelve MCSs observed in the case studies followed a pattern in which the convective rain area peaked first, followed by a peak in stratiform rain area, then a peak in mixed anvil area typically lagging 1–2 h behind the stratiform rain area peak, and finally ice anvil area peak occurring 1–3 h after a mixed anvil
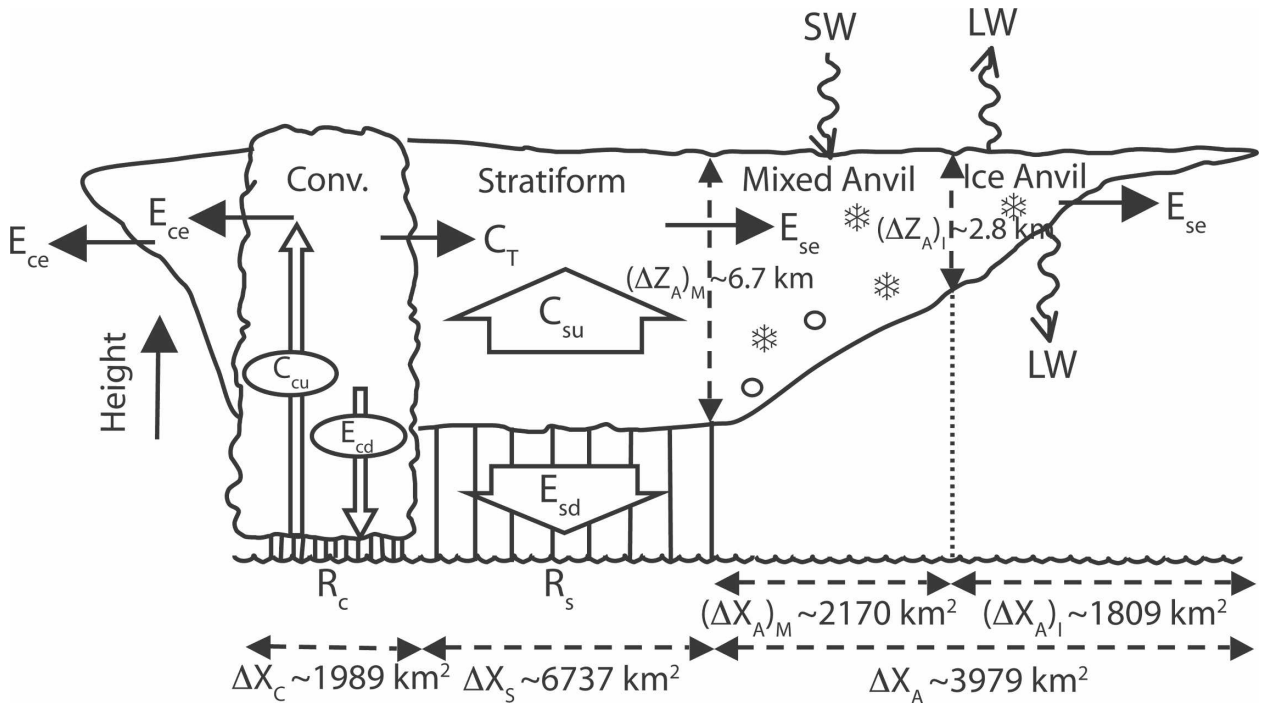
FIG. 17. Same as Fig. 1 but with the average rain and anvil areas and anvil thickness from TWP-ICE C-POL observations. The area of the radar domain is 45 216 km^2.

area peak. Five convective systems were isolated enough to observe the longevity of the anvil. During these systems, anvil typically lasted 4–10 h after the initial convective rain area peak. Understanding the interaction between the anvil and the rest of the precipitating system will lead to more realistic numerical representations of anvil properties associated with deep convection in the tropics.

Information about the evolution of the anvil could lead to a better understanding of what sustains the anvil. A strong positive correlation between ice anvil area and thickness and a strong negative correlation between ice anvil thickness and height was found throughout the entire experiment (with the exception of the active monsoon). These correlations most likely result from sedimentation occurring in the anvil over time. During the lifetime of the anvil, as more hydrometeors collect aloft (increasing anvil areal coverage), larger particles fall out of the anvil first, evaporating and moistening the atmosphere underneath the anvil. Once the smaller particles fall out, they do not evaporate due to the moister environment beneath the anvil. This sedimentation process creates a lower base and thicker anvil.

During the entire experiment (except the active monsoon) ice anvil bottom varied significantly more than ice anvil top. Several explanations were proposed for this, the most likely being that the anvil top is located around the level of neutral buoyancy where it is not free to penetrate above that level. Another possible cause is larger amounts of IWC in the base of the anvil causing greater radiative destabilization due to more absorption and extinction of radiation in the larger particles. Sedimentation would also be a factor leading to a more variable ice anvil bottom.

Based on estimates from the Tropical Rainfall Measuring Mission (TRMM) precipitation radar, the average annual latent heating over Darwin is 2–3 K day^{-1} at 400 hPa (Schumacher et al. 2004). If we assume that anvil can have a local radiative heating rate of 10 K day^{-1} and use the fact that mixed and ice anvil each covered almost 5% of the radar domain during TWP-ICE, the heating from the anvil observable by C-POL may increase the total heating associated with monsoon cloud systems by ~0.5 K day^{-1} at upper levels, a non-negligible amount compared to the average annual latent heating. In addition, the area coverage by ice anvil is an underestimate since C-POL is not able to sense thinner anvil and cirrus. Regardless, the radiative heating associated with anvil at upper levels would be expected to enhance circulations such as the Hadley or Walker circulations (Randall et al. 1989; Slingo and Slingo 1991; Sherwood et al. 1994). Hartmann et al. (1984) found a larger midlatitude circulation response

with an elevated heating profile. Therefore, it is expected that the radiative heating during the active monsoon would have important impacts on tropical–extratropical interactions.

REFERENCES

Ackerman, T. P., K.-N. Liou, F. P. J. Valero, and L. Pfister, 1988: Heating rates in tropical anvils. *J. Atmos. Sci.,* **45,** 1606–1623.

Bergman, J. W., and H. H. Hendon, 2000: Cloud radiative forcing of the low-latitude tropospheric circulation: Linear calculations. *J. Atmos. Sci.,* **57,** 2225–2245.

Bringi, V. N., G. Huang, V. Chandrasekar, and T. D. Keenan, 2001: An areal rainfall estimator using differential propagation phase: Evaluation using a C-band radar and a dense gauge network in the tropics. *J. Atmos. Oceanic Technol.,* **18,** 1810–1818.

Churchill, D. D., and R. A. Houze Jr., 1984: Mesoscale updraft magnitude and cloud-ice content deduced from the ice budget of the stratiform region of a tropical cloud cluster. *J. Atmos. Sci.,* **41,** 1717–1725.

Comstock, J. M., T. P. Ackerman, and G. G. Mace, 2002: Ground-based lidar and radar remote sensing of tropical cirrus clouds at Nauru Island: Cloud statistics and radiative impacts. *J. Geophys. Res.,* **107,** 4714, doi:10.1029/2002JD002203.

Folkins, I., 2002: Origin of lapse rate changes in the upper tropical troposphere. *J. Atmos. Sci.,* **59,** 992–1005.

Gamache, J. F., and R. A. Houze Jr., 1983: Water budget of a mesoscale convective system in the tropics. *J. Atmos. Sci.,* **40,** 1835–1850.

Hartmann, D. L., H. H. Hendon, and R. A. Houze Jr., 1984: Some implications of the mesoscale circulations in tropical cloud clusters for large-scale dynamics and climate. *J. Atmos. Sci.,* **41,** 113–121.

Hastenrath, S., 1991: *Climate Dynamics of the Tropics.* Kluwer Academic, 488 pp.

Heymsfield, A. J., and L. M. Miloshevich, 1995: Relative humidity and temperature influences on cirrus formation and evolution: Observations from wave clouds and FIRE II. *J. Atmos. Sci.,* **52,** 4302–4326.

Houze, R. A., Jr., 1982: Cloud clusters and large-scale vertical motions in the tropics. *J. Meteor. Soc. Japan,* **60,** 396–410.

——, 1993: *Cloud Dynamics.* Academic Press, 573 pp.

——, 1997: Stratiform precipitation in regions of convection: A meteorological paradox? *Bull. Amer. Meteor. Soc.,* **78,** 2179–2196.

——, C.-P. Cheng, C. A. Leary, and J. F. Gamache, 1980: Diagnosis of cloud mass and heat fluxes from radar and synoptic data. *J. Atmos. Sci.,* **37,** 754–773.

——, S. Brodzik, C. Schumacher, S. E. Yuter, and C. R. Williams, 2004: Uncertainties in oceanic radar rain maps at Kwajalein and implications for satellite validation. *J. Appl. Meteor.,* **43,** 1114–1132.

Keenan, T., K. Glasson, F. Cummings, T. S. Bird, J. Keeler, and J. Lutz, 1998: The BMRC/NCAR C-band polarimetric (C-POL) radar system. *J. Atmos. Oceanic Technol.,* **15,** 871–886.

Leary, C. A., and R. A. Houze Jr., 1980: The contribution of mesoscale motions to the mass and heat fluxes of an intense tropical convective system. *J. Atmos. Sci.,* **37,** 784–796.

Lilly, D. K., 1988: Cirrus outflow dynamics. *J. Atmos. Sci.,* **45,** 1594–1605.

Liou, K. N., 2002: *An Introduction to Atmospheric Radiation.* 2nd ed. Academic Press, 583 pp.

Mace, G. G., M. Deng, B. Soden, and E. Zisper, 2006: Association of tropical cirrus in the 10–15-km layer with deep convective sources: An observational study combining millimeter radar data and satellite-derived trajectories. *J. Atmos. Sci.,* **63,** 480–503.

Massie, S., A. Gettelman, W. Randel, and D. Baumgardner, 2002: Distribution of tropical cirrus in relation to convection. *J. Geophys. Res.,* **107,** 4591, doi:10.1029/2001JD001293.

McFarquhar, G. M., and A. J. Heymsfield, 1996: Microphysical characteristics of three anvils sampled during the Central Equatorial Pacific Experiment. *J. Atmos. Sci.,* **53,** 2401–2423.

McGill, M. J., D. L. Hlavka, W. D. Hart, E. J. Welton, and J. R. Campbell, 2003: Airborne lidar measurements of aerosol optical properties during SAFARI-2000. *J. Geophys. Res.,* **108,** 8493, doi:10.1029/2002JD002370.

Mullendore, G. L., D. R. Durran, and J. R. Holton, 2005: Cross-tropopause tracer transport in midlatitude convection. *J. Geophys. Res.,* **110,** D06113, doi:10.1029/2004JD005059.

Petre, J. M., and J. Verlinde, 2004: Cloud radar observations of Kelvin–Helmholtz instability in a Florida anvil. *Mon. Wea. Rev.,* **132,** 2520–2523.

Randall, D. A., Harshvardhan, D. A. Dazlich, and T. G. Corsetti, 1989: Interactions among radiation, convection, and large-scale dynamics in a general circulation model. *J. Atmos. Sci.,* **46,** 1943–1970.

Schumacher, C., R. A. Houze Jr., and I. Kraucunas, 2004: The tropical dynamical response to latent heating estimates derived from the TRMM precipitation radar. *J. Atmos. Sci.,* **61,** 1341–1358.

Sherwood, S. C., V. Ramanathan, T. P. Barnett, M. K. Tyree, and E. Roeckner, 1994: Response of an atmospheric general circulation model to radiative forcing of tropical clouds. *J. Geophys. Res.,* **99,** 20 829–20 846.

Slingo, A., and J. M. Slingo, 1991: Response of the National Center for Atmospheric Research Community Climate Model to improvements in the representation of clouds. *J. Geophys. Res.,* **96,** 15 341–15 357.

Steiner, M., R. A. Houze Jr., and S. E. Yuter, 1995: Climatological characterization of three-dimensional storm structure from operational radar and rain gauge data. *J. Appl. Meteor.,* **34,** 1978–2007.

Webster, P. J., and G. L. Stephens, 1980: Tropical upper-tropospheric extended clouds: Inferences from Winter MONEX. *J. Atmos. Sci.,* **37,** 1521–1541.